

# Multiphysics topology optimization for piezoelectric acoustic focuser

Gil Ho Yoon<sup>a,\*</sup>, Hyunggyu Choi<sup>a</sup>, Shin Hur<sup>b</sup>

<sup>a</sup> School of Mechanical Engineering, Hanyang University, Seoul, Republic of Korea

<sup>b</sup> Korea Institute of Machinery & Materials 156 Gajeongbuk-Ro, Yuseong-Gu, Daejeon, Republic of Korea

Received 2 June 2017; received in revised form 30 November 2017; accepted 1 December 2017

Available online 26 December 2017

## Highlights

- The multiphysics simulation for acoustic focuser topological design is performed.
- Optimal numbers and locations of rings are found by topology optimization.
- The manufacturing constraint is imposed by the modified density filter.
- The obtained designs show superior performance on the energy focusing.
- The designs are sensitive to optimization formulations.

## Abstract

The application of piezoelectric materials allows many advantages such as reducing the number of parts and manufacturing cost of a mechanical system. Despite these merits, the performance predictions and optimization of piezoelectric-material-based devices are challenging because of the mutual coupling between electricity and mechanics. The analysis and the optimization become more challenging when acoustics are to be coupled with piezoelectric-material-based devices. In the present study, the mutual couplings among electric, mechanics, and acoustics are simulated and its applications for the topology optimization of an acoustic energy focuser are presented. Owing to the local optima issue, some blurred and unsuccessful layouts are obtained. To overcome this issue and impose the manufacturing constraint, a modified morphology density filter is also developed. With the presented approach, it is possible to determine some optimized piezoelectric rings to focus acoustic energy. Compared with the existing design methods, some better designs in terms of objective value can be obtained by the present approach.

© 2017 Published by Elsevier B.V.

**Keywords:** Topology optimization; Piezoelectric material; SIMP approach; Acoustic focuser; Manufacturing constraint

\* Corresponding author.

E-mail addresses: [ghy@hanyang.ac.kr](mailto:ghy@hanyang.ac.kr), [gilho.yoon@gmail.com](mailto:gilho.yoon@gmail.com) (G.H. Yoon).

## 1. Introduction

This study presents a new topology optimization (TO) scheme for the optimized ring design of a piezoelectric-based acoustic focuser in the framework of the multiphysics finite element method, in which electric, mechanical deformation, and acoustic pressure are the primal variables. There are many innovative engineering devices with man-made piezoelectric materials and the research about piezoelectric materials has gained considerable importance in the development of energy harvesting devices, hearing aid devices, speakers, and acoustic energy focusers [1–8]. However, it is challenging to intuitively predict and optimize the performances of piezoelectric devices, considering the mutual coupling between electric and mechanical systems. The difficulty is more profound with the mutual coupling to an acoustic system. Therefore, the TO method can be advantageous in an acoustic–electro–mechanical coupling system, as it can play as a black-box design tool providing optimized topologies by minimizing or maximizing a given objective function, subject to certain engineering constraints [1–8]. This research develops a new application for the design of an efficient piezoelectric acoustic focuser with the multiphysics analysis of acoustic, electric, and mechanical systems.

### 1.1. Piezoelectric material and optimization

Piezoelectric materials have attracted considerable academic and industrial interest, owing to their piezoelectricity and reverse piezoelectricity in Fig. 1 [1]. These interesting material properties originate from the alteration in the polarization direction [1]; the polarized molecules align parallel to electric field and some mechanical actuations can be obtained. This interesting property is used to harvest electric energy or make sensors and actuators [7,9,10].

There has also been relevant research into the optimizations of piezoelectric devices.

There is some relevant research into the structural optimization with piezoelectric materials (see [11,12] for general optimization). In [13], the compliant mechanical amplifiers for piezoelectric actuators are optimized by TO. In [14,15], the placement of piezoelectric material is optimized by TO. In [16], a multi-actuated functionally graded piezoelectric design is proposed. In [8,17], the optimal shape and topology for an optimal energy harvester are found by the level set-based method. In [18], the simultaneous structural TO for electromagnetic sources and ferromagnetic material was proposed. In [19], the electro shape is optimized by TO. In [20], multiphysics interpolation scheme was proposed for piezoelectric systems. In [21], the design of a piezoelectric plane and shell actuators was proposed. In [2], a TO approach for multilayer plates and shells was proposed. The TO for a transducer was proposed in [3–5] and the flexensional actuator was optimized in [6]. In [22], the thickness of the base structure and the location of piezoelectric sensor and actuator as well as control gains are optimized for the sound radiation. Rather than a static load, dynamic loads are also considered to maximize the energy conversion in [23] and [24]. Here, it is noteworthy that the optimized design of an acoustic energy focuser requires the multiphysics analysis, as shown in Fig. 2.

### 1.2. Acoustic energy focuser and topology optimization

Much scientific and engineering research into focusing acoustic energy has been undertaken for various engineering and medical applications, such as nondestructive testing techniques that inspect structures for internal hidden flaws or energy focusing to kill cancer cells. For these interesting applications, piezoelectric devices are commonly used because of the simplicity of manufacturing and the accurate and easy controllability. In addition to engineering applications, the acoustic energy focuser is also applied for medical therapeutic purposes. In obstetrics and gynecology, ultrasound waves excited by piezoelectric material are capable of transmitting energy to obtain medical images of a fetus inside its mother's body. Another example is to heat tumors or break kidney stones by focused ultrasound.

In order to focus acoustic energy simply, ultrasonic focusing lenses, such as a spherical lens, reflection wall, Fresnel lens, and self-focusing acoustic-wave liquid ejector have been proposed [25,26]. Among these, the Fresnel lens with repeated flat annular piezoelectric rings shows advantages of planar geometry (not bulky), and it is reported that it is relatively easy to fabricate but the geometry is critical in terms of the efficiency. Owing to higher-order diffraction, the Fresnel PT lens has some difficulties to concentrate the acoustic energy. It was commented that some unwanted energy focusing spots are observed with un-tuned Fresnel equal-spaced PT rings. Thus, it is necessary to develop an optimization framework to achieve arbitrarily designed focal pattern along the axis. One of the possible optimization approaches is the *size optimization*, optimizing the focal pattern by changing the radii of the PT rings. However, the

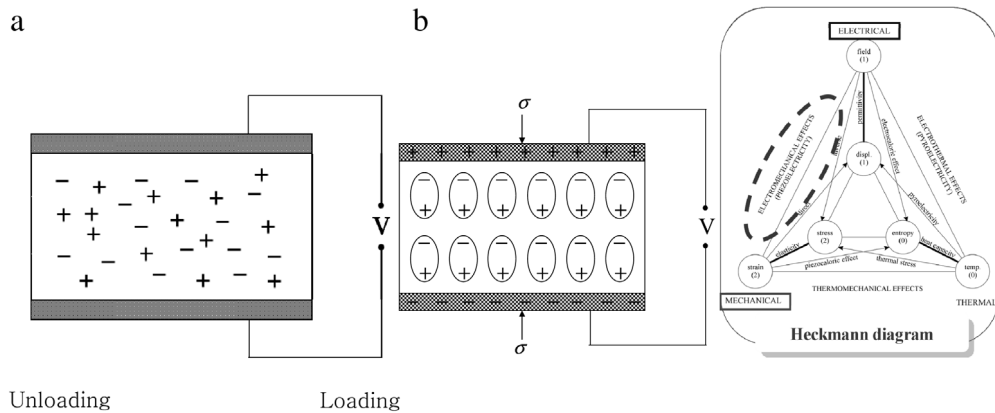


**Fig. 1.** (a) Piezoelectric phenomenon, and (b) Heckmann diagram.

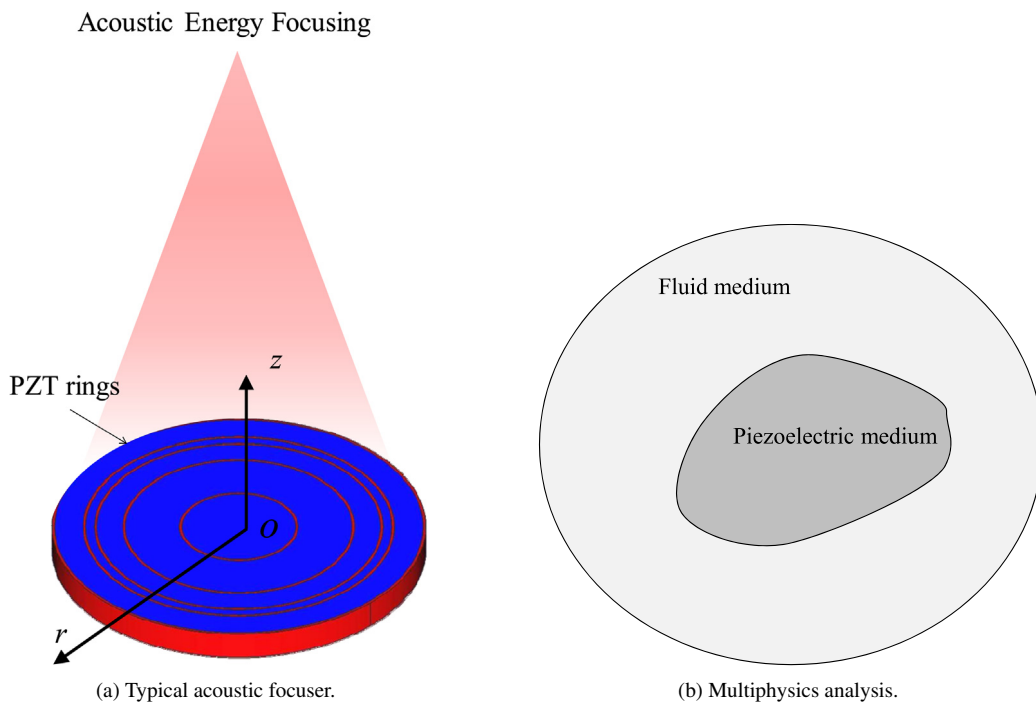


**Fig. 2.** (a) Schematics of the configurable planar metasurface PT prototype [25,26] and (b) the multiphysics analysis domain (Piezoelectric domain and fluid domain).

optimization formulation depending on the type of objective and constraint functions can have many multiple local optima and it is very difficult to apply.

This study develops the TO method for the optimized design of an acoustic energy focuser based on the solid isotropic material with penalization (SIMP) approach. To the best of our knowledge, few studies on TO have considered multiphysics analysis of acoustic, electric, and mechanical systems [12,27–29]. Most of the relevant studies have considered the coupling between electric and mechanical systems for energy harvesting and there are the studies considering the multiphysics analysis of simplified acoustic, electric and mechanical systems. Indeed, this paper focuses on the development of a new TO theory by considering the multiphysics analysis.

The remainder of this paper is organized as follows. Section 2 presents the theory and FE formulation of the multiphysics system. Sections 3 and 4 present several optimization formulations for the acoustic energy focuser, the optimization results, and some physical interpretations of the obtained designs. Finally, Section 5 summarizes the findings and discusses possible future works.

## 2. Finite element formulation for multiphysics system (acoustic, electric, and mechanical systems)

### 2.1. Piezoelectric simulation

Commonly, the following electromechanical coupling phenomena between the mechanical and electrical domains are employed:

$$\mathbf{T} = \mathbf{c}^E \mathbf{S} - \mathbf{e} \mathbf{E}, \mathbf{D} = \mathbf{e}^T \mathbf{S} + \boldsymbol{\epsilon}^S \mathbf{E} \quad (1a)$$

$$\mathbf{c}^E = \begin{bmatrix} 1.27 \times 10^{11} & 8.02 \times 10^{11} & 8.47 \times 10^{11} & 0 & 0 & 0 \\ & 1.27 \times 10^{11} & 8.47 \times 10^{11} & 0 & 0 & 0 \\ & & 1.17 \times 10^{11} & 0 & 0 & 0 \\ & & & 2.30 \times 10^{10} & 0 & 0 \\ & & & & 2.30 \times 10^{10} & 0 \\ & & & & & 2.35 \times 10^{10} \end{bmatrix} [\text{Pa}] \quad (1b)$$

$$\mathbf{e} = \begin{bmatrix} 0 & 0 & 0 & 0 & 17.0345 & 0 \\ 0 & 0 & 0 & 17.0345 & 0 & 0 \\ -6.62281 & -6.2281 & 23.2403 & 0 & 0 & 0 \end{bmatrix} [\text{C/m}^2] \quad (1c)$$

$$\boldsymbol{\epsilon}^S / \epsilon_a = \begin{bmatrix} 1704.4 & 0 & 0 \\ 0 & 1704.4 & 0 \\ 0 & 0 & 1433.6 \end{bmatrix} (\epsilon_a = 8.854 \times 10^{-12}) \quad (1d)$$

$$\rho = 7500 [\text{kg/m}^3] \quad (1e)$$

where the mechanical stress and strain are denoted by  $\mathbf{T}$  and  $\mathbf{S}$ , respectively, and the electric displacement and electric field are denoted by  $\mathbf{D}$  and  $\mathbf{E}$ , respectively. We assume the material linearity for the linear stiffness matrix  $\mathbf{c}^E$  (also called the stiffness tensor), piezoelectric matrix  $\mathbf{e}$ , and permittivity matrix  $\boldsymbol{\epsilon}^S$  in (1). The PZT-5H material is considered [25]. The material properties are well defined. The 2-D axisymmetric equations can be derived by setting tangential components as well as derivatives with respect to the angular variable to zeros from the 3D equations in cylindrical coordinates [30]. The axis of the cylinder coincides with the axis  $z$ , the radius, polar angle, and axial coordinate are  $r$ ,  $\theta$ , and  $z$ , respectively. The radial, tangential and axial displacements are  $u_r$ ,  $u_\theta$ , and  $u_z$ , respectively. The mechanical strain tensor is defined by

$$\mathbf{S} = \frac{1}{2}(\nabla \mathbf{U} + \nabla \mathbf{U}^T) \text{ or } \begin{bmatrix} e_{rr} \\ e_{zz} \\ e_{\theta\theta} \\ \gamma_{rz} \end{bmatrix} = \begin{bmatrix} \partial/\partial r & 0 \\ 0 & \partial/\partial z \\ 1/r & 0 \\ \partial/\partial z & \partial/\partial r \end{bmatrix} \begin{bmatrix} u_r \\ u_z \end{bmatrix}. \quad (2)$$

The mechanical displacements are  $\mathbf{U}$ . The electric field is derivable from the scalar electric potential  $\Phi$ .

$$\mathbf{E} = -\nabla \Phi \text{ or } E_{rr} = -\frac{\partial \Phi}{\partial r}, E_{\theta\theta} = -\frac{\partial \Phi}{r \partial \theta}, E_{zz} = -\frac{\partial \Phi}{\partial z}. \quad (3)$$

The equation of motion for a piezoelectric medium can be written as follows

$$\nabla \cdot \mathbf{T} = \rho \ddot{\mathbf{U}}. \quad (4)$$

The FE procedure can be developed with the displacements ( $\mathbf{u}$ ) and potential ( $\varphi$ ) as the primary (unknown) FE variables as follows [10,31,32]:

$$\left\{ -\omega^2 \begin{bmatrix} \mathbf{M} & \mathbf{0} \\ \mathbf{0} & \mathbf{0} \end{bmatrix} + \begin{bmatrix} \mathbf{K}_{uu} & \mathbf{K}_{u\varphi} \\ \mathbf{K}_{\varphi u} & -\mathbf{K}_{\varphi\varphi} \end{bmatrix} \right\} \begin{bmatrix} \mathbf{u} \\ \varphi \end{bmatrix} = \begin{bmatrix} \mathbf{F} \\ \mathbf{Q} \end{bmatrix} \quad (5)$$

$$\mathbf{M} = \sum_{e=1}^{NE} \mathbf{m}_{uu}^e, \mathbf{m}_{uu}^e = \int_{\Omega_e} \rho \mathbf{H}_u^T \mathbf{H}_u d\mathbf{v} \quad (6)$$

$$\mathbf{K}_{uu} = \sum_{e=1}^{NE} \mathbf{K}_{uu}^e, \mathbf{K}_{u\varphi} = \sum_{e=1}^{NE} \mathbf{K}_{u\varphi}^e \quad (7)$$

$$\mathbf{K}_{\varphi u} = \sum_{e=1}^{NE} \mathbf{K}_{\varphi u}^e, \mathbf{K}_{\varphi\varphi} = \sum_{e=1}^{NE} \mathbf{K}_{\varphi\varphi}^e \quad (8)$$

$$\mathbf{K}_{uu}^e = \int_{\Omega_e} \mathbf{B}_u^T \mathbf{c}^E \mathbf{B}_u d\mathbf{v}, \mathbf{K}_{u\varphi}^e = \int_{\Omega_e} \mathbf{B}_u^T \mathbf{e} \mathbf{B}_{\varphi} d\mathbf{v}, \mathbf{K}_{\varphi u}^e = \int_{\Omega_e} \mathbf{B}_{\varphi}^T \mathbf{e}^T \mathbf{B}_u d\mathbf{v}, \mathbf{K}_{\varphi\varphi}^e = \int_{\Omega_e} \mathbf{B}_{\varphi}^T \boldsymbol{\epsilon}^S \mathbf{B}_{\varphi} d\mathbf{v}$$

where the global mass matrix is  $\mathbf{M}$  and the global structural stiffness matrix and the global potential stiffness matrix are  $\mathbf{K}_{uu}$  and  $\mathbf{K}_{\varphi\varphi}$ , respectively. The coupling matrix between the mechanical displacements and the electric potential is  $\mathbf{K}_{u\varphi}$  ( $\mathbf{K}_{\varphi u} = \mathbf{K}_{u\varphi}^T$ ). The total number of finite elements is  $NE$ . The matrices for the  $e$ th element have the right-upper script  $e$ . The 2nd order shape function and the strain–displacement matrix for the mechanical displacements are  $\mathbf{H}_u$  and  $\mathbf{B}_u$ , and the 2nd order electric field–potential matrix is  $\mathbf{B}_{\varphi}$ . (See [33,34] for more details.)

## 2.2. Acoustic simulation

Acoustic pressure propagation in a homogeneous acoustic medium by neglecting the dissipation of acoustic energy is normally simulated by solving the following Helmholtz equation with proper boundary conditions assuming harmonically varying pressure, i.e.,  $\tilde{p}(t) = p e^{i\omega t}$ .

$$\text{Helmholtz equation : } \nabla \cdot \left( \frac{1}{\rho_a} \nabla p \right) + \frac{\omega^2 p}{\rho_a c_a^2} = 0, \left( k = \frac{\omega}{c_a} \right) \quad \text{on the acoustic domain } \Omega_a \quad (9)$$

where  $p$ ,  $\rho_a$ , and  $c_a$  are the acoustic pressure in  $\Omega_a$ , air density, and local speed of sound, respectively. The del operator is defined by  $\nabla = \left[ \frac{\partial}{\partial r}, \frac{\partial}{r\partial\theta}, \frac{\partial}{\partial z} \right]$  and the Laplace operator in the axisymmetric system is defined by  $\nabla^2 = \frac{\partial}{r\partial r} \left( r \frac{\partial}{\partial r} \right) + \frac{\partial^2}{\partial z^2}$ . The angular velocity and the wave number are denoted by  $\omega$  and  $k$ , respectively. For the FE simulation, the pressure  $p$  and its spatial differential  $\nabla p$  are approximated by the nodal pressure values as (10). The column vector of the nodal pressures in the  $e$ th element, the 2nd order shape function matrix, and the differentiated shape function matrix are denoted by  $\mathbf{p}_e$ ,  $\mathbf{N}$ , and  $\mathbf{B}$ , respectively. The FE matrix equations in (11) and (13) are obtained by the discretization in (10).

$$p \approx \mathbf{N} \mathbf{p}_e, \nabla p \approx \mathbf{B} \mathbf{p}_e \quad (10)$$

$$\int_{\Omega_a} \frac{1}{\rho} \mathbf{B}^T \mathbf{B} \mathbf{p}_e d\Omega - \int_{\Omega_a} \frac{\omega^2}{\rho c^2} \mathbf{N}^T \mathbf{N} \mathbf{p}_e d\Omega = -i\omega \int_{\Gamma} \frac{1}{\rho c} \mathbf{N}^T \mathbf{N} \mathbf{p}_e d\Gamma \quad (11)$$

$$[\mathbf{K}_a - \omega^2 \mathbf{M}_a + i\omega \mathbf{F}^{radiation}] \mathbf{p} = 0, \mathbf{M}_a = \sum_{e=1}^{NEA} \mathbf{m}_p^e, \mathbf{K}_a = \sum_{e=1}^{NEA} \mathbf{k}_p^e, \mathbf{F}^{radiation} = \sum_{e=1}^{NEA} \mathbf{f}_e^{radiation} \quad (12)$$

$$\mathbf{k}_p^e = \frac{1}{\rho_e} \int_{\Omega_e} \mathbf{B}^T \mathbf{B} d\Omega, \quad \mathbf{m}_p^e = \frac{1}{\rho_e c_e^2} \int_{\Omega_e} \mathbf{N}^T \mathbf{N} d\Omega, \quad \mathbf{f}_e^{radiation} = \frac{1}{\rho_e c_e} \int_{\Gamma_e} \mathbf{c} \mathbf{N}^T \mathbf{N} d\Gamma. \quad (13)$$

In (13),  $\mathbf{k}_p^e$  and  $\mathbf{m}_p^e$  are defined as local stiffness and mass for the  $e$ th element, respectively. The acoustic element is denoted by  $NEA$ . The density, wave speed, domain, and boundary of the  $e$ th element are defined as  $\rho_e$ ,  $c_e$ ,  $\Omega_e$ , and  $\Gamma_e$ , respectively; if we assume an isotropic acoustic medium, the acoustic density and the acoustic wave speed of the  $e$ th element become  $\rho_e = \rho_a = 1.25 \text{ kg/m}^3$  and  $c_e = c_a = 343 \text{ m/s}$ , respectively. These local matrices are assembled into the global matrices for the entire domain. Note that the force matrix,  $\mathbf{f}_e^{radiation}$ , is superposed only for the elements in the acoustic boundary. The final governing equation is summarized as (12). The superposed global matrices for the local matrices  $\mathbf{k}_e$ ,  $\mathbf{m}_e$ , and  $\mathbf{f}_e^{radiation}$  are denoted by  $\mathbf{K}_a$ ,  $\mathbf{M}_a$ , and  $\mathbf{F}^{radiation}$ , respectively.

### 2.3. Interface simulation

The interfacing boundary conditions between the acoustic domain and structural domain can be derived from the continuum equation of fluid, which actually moves due to acoustic pressure. For the acoustic domain, the local balance of linear momentum equation should be satisfied as follows:

$$\text{Interface condition for acoustic domain : } \mathbf{n} \cdot \nabla p = \omega^2 \rho_a \mathbf{n}^T \mathbf{u} \text{ in } S_{int} \quad (14)$$

where  $S_{int}$  is the interfacing boundary and the outgoing normal vector is denoted by  $\mathbf{n}$ . The structural displacement at the interaction boundary is denoted by  $\mathbf{u}$ . At the interface of the structural domain, the traction of the solid part should equal the pressure and the following condition should be imposed.

$$\text{Interface condition for the solid part : } \mathbf{f}_{S_{int}} = \mathbf{n} \cdot p \text{ on } S_{int}. \quad (15)$$

The structural force applied at the interaction boundary is denoted by  $\mathbf{f}_{S_{int}}$ . After imposing the interface boundary conditions of Eqs. (14) and (15), the scattering wave and the structural response can be calculated by a standard finite element procedure. The entire procedure above with the interaction boundary conditions is represented in Fig. 3. (See [34] for more details.) The local fluid–structure coupling matrix for the  $e$ th element is defined by

$$\mathbf{C}_{up}^e = \int_{\Gamma_I^e} \rho_f \mathbf{N}_u^T \mathbf{n} \mathbf{N}_p d\Gamma, \quad \mathbf{C}_{up} = \sum_{e=1}^{CNE} \mathbf{C}_{up}^e \quad (16)$$

where the normal vector,  $\mathbf{n}$  pointing into the fluid, is defined at the surface  $\Gamma_I^e$  where the number of coupling elements is denoted by  $CNE$ . The global coupling matrix is defined summing the above coupling matrix. Considering the couplings, the total system matrices can be written as follows:

$$\begin{aligned} \mathbf{R}(\mathbf{S}) = & \left\{ -\omega^2 \begin{bmatrix} \mathbf{M} & \mathbf{0} & \mathbf{0} \\ \mathbf{0} & \mathbf{0} & \mathbf{0} \\ \mathbf{0} & \mathbf{0} & \mathbf{M}_a \end{bmatrix} + i\omega \begin{bmatrix} \mathbf{0} & \mathbf{0} & \mathbf{C}_{up} \\ \mathbf{0} & \mathbf{0} & \mathbf{0} \\ -\mathbf{C}_{up}^T & \mathbf{0} & \mathbf{F}^{radiation} \end{bmatrix} + \begin{bmatrix} \mathbf{K}_{uu} & \mathbf{K}_{u\varphi} & \mathbf{0} \\ \mathbf{K}_{\varphi u} & -\mathbf{K}_{\varphi\varphi} & \mathbf{0} \\ \mathbf{0} & \mathbf{0} & \mathbf{K}_a \end{bmatrix} \right\} \\ & \times \begin{bmatrix} \mathbf{u} \\ \varphi \\ \mathbf{p} \end{bmatrix} - \begin{bmatrix} \mathbf{F} \\ \mathbf{Q} \\ \mathbf{0} \end{bmatrix} = \mathbf{0}, (\mathbf{S} = \begin{bmatrix} \mathbf{u} \\ \varphi \\ \mathbf{p} \end{bmatrix}) \end{aligned} \quad (17)$$

where the residual vector and the state variables are denoted by  $\mathbf{R}$  and  $\mathbf{S}$ , respectively.

## 3. Topology optimization formulation for acoustic energy focuser

### 3.1. Optimization formulation

The piezo rings are distributed in the three-dimensional view of an illustrative acoustic focuser in Fig. 1. In the present study, a ceramic-based piezoelectric material PZT-5H is numerically modeled. It is assumed that the heights of the piezo rings are equal, and the SIMP design variables of the topology optimization are assigned to each finite element in the domain modeled for the piezo rings. The PZT domain is discretized by 3000 by 10 finite elements and the acoustic domain is discretized to have at least 5 elements per wavelength. We mathematically modeled the domains with ones for the design variables as the piezoelectric domain and the domain with small values as the void domains. For the numerical analysis, the axisymmetric finite element theory is implemented and the mutual coupling is made between the acoustic domain (a quarter sphere) and the piezoelectric domain. Then, an optimal topology maximizing the objective function with some constraints should be obtained by the TO formulation.

For a TO formulation, the following problem can be considered.

$$\begin{aligned} & \text{Max } \int_{\Omega_{obj}} |p| dv (\Omega_{obj} : \text{an objective domain}) \\ & \text{Subject to } \sum_{e=1}^{NED} \gamma_e v_e \leq V^* \\ & \tilde{\gamma} = \text{filter}(\gamma), 0.001 \leq \gamma_e \leq 1 \end{aligned} \quad (18)$$

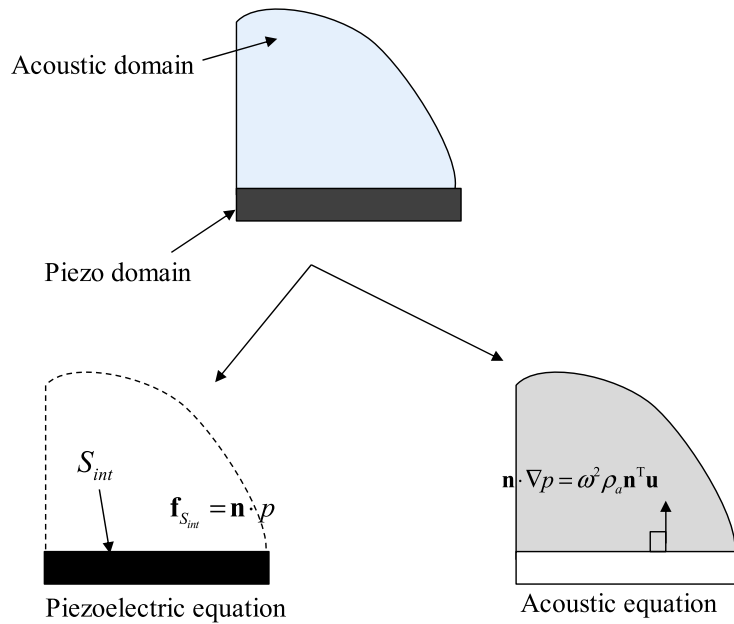


**Fig. 3.** Governing equations and the interaction boundary conditions between acoustic and structural domains.

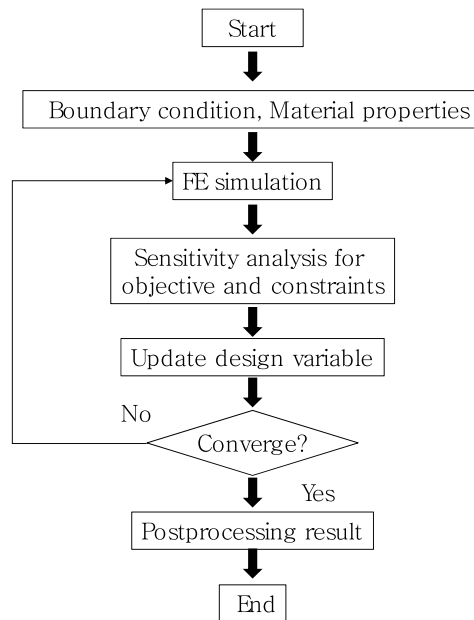


**Fig. 4.** Topology design optimization procedure.

where the design variable and the volume of the  $e$ th element are denoted by  $\gamma_e$  and  $v_e$ , respectively. The upper bound of the mass constraint is  $V^*$  and the number of design variables is  $NED$ . The constraint is inserted to efficiently use the piezoelectric material and to regularize the TO formulation. Physically, we noticed that the mass constraint has a limited meaning because the etching technique removing the piezoelectric material is often used. However, in our tests, it helps us to find out an optimized topology. For the sensitivity analysis, the adjoint variable method is employed. The optimization procedure shown in Fig. 4 is implemented with the method of moving asymptotes (MMA) [35] for an optimization algorithm.

### 3.1.1. Sensitivity analysis

For the analytical sensitivity analysis, the adjoint variable method is employed. For the simple notations, the vector of the state variables of structural displacements, potential, and acoustic is denoted by  $\mathbf{S}$ . For an objective function,  $\phi$ , the sensitivity value can be defined with the Lagrange multipliers  $\lambda$  and  $\lambda_{im}$ .

$$L = \phi + \lambda^T \mathbf{R} + \lambda_{im}^T \bar{\mathbf{R}} \quad (19)$$

where the residual vector of the governing equation is denoted by  $\mathbf{R}$  and the conjugate residual is  $\bar{\mathbf{R}}$ . The derivatives of  $L$  with respect to the design variable are summarized as follows:

$$\begin{aligned} \frac{dL}{d\gamma} &= \frac{\partial \phi}{\partial \gamma} + \lambda^T \left( \frac{\partial \mathbf{R}}{\partial \gamma} \right) + \left( \frac{\partial \phi}{\partial \mathbf{S}} + \lambda^T \frac{\partial \mathbf{R}}{\partial \mathbf{S}} \right) \frac{d\mathbf{S}}{d\gamma} + \lambda_{im}^T \left( \frac{\partial \bar{\mathbf{R}}}{\partial \gamma} \right) + \left( \frac{\partial \phi}{\partial \bar{\mathbf{S}}} + \lambda_{im}^T \frac{\partial \bar{\mathbf{R}}}{\partial \bar{\mathbf{S}}} \right) \frac{d\bar{\mathbf{S}}}{d\gamma} \\ \frac{dL}{d\gamma} &= \frac{\partial \phi}{\partial \gamma} + \lambda^T \left( \frac{\partial \mathbf{R}}{\partial \gamma} \right) + \lambda_{im}^T \left( \frac{\partial \bar{\mathbf{R}}}{\partial \gamma} \right). \end{aligned} \quad (20)$$

The last term in Eq. (20) can be eliminated with the Lagrange multipliers in (21).

$$\frac{\partial \phi}{\partial \mathbf{S}} + \lambda^T \frac{\partial \mathbf{R}}{\partial \mathbf{S}} = \mathbf{0}, \quad \frac{\partial \phi}{\partial \bar{\mathbf{S}}} + \lambda_{im}^T \frac{\partial \bar{\mathbf{R}}}{\partial \bar{\mathbf{S}}} = \mathbf{0} \quad (21)$$

$$\frac{\partial \mathbf{R}}{\partial \mathbf{S}} = -\omega^2 \begin{bmatrix} \mathbf{M} & \mathbf{0} & \mathbf{0} \\ \mathbf{0} & \mathbf{0} & \mathbf{0} \\ \mathbf{0} & \mathbf{0} & \mathbf{M}_a \end{bmatrix} + i\omega \begin{bmatrix} \mathbf{0} & \mathbf{0} & \mathbf{C}_{up} \\ \mathbf{0} & \mathbf{0} & \mathbf{0} \\ -\mathbf{C}_{up}^T & \mathbf{0} & \mathbf{F}^{radiation} \end{bmatrix} + \begin{bmatrix} \mathbf{K}_{uu} & \mathbf{K}_{u\varphi} & \mathbf{0} \\ \mathbf{K}_{\varphi u} & -\mathbf{K}_{\varphi\varphi} & \mathbf{0} \\ \mathbf{0} & \mathbf{0} & \mathbf{K}_a \end{bmatrix}. \quad (22)$$

The terms,  $\frac{\partial \mathbf{R}}{\partial \mathbf{S}}$  and  $\frac{\partial \bar{\mathbf{R}}}{\partial \bar{\mathbf{S}}}$ , becomes the tangent stiffness matrices of the nonlinear governing equations.

### 3.1.2. Manufacturing constraint: regulation or restriction

Furthermore, it is important to consider manufacturing issues for a successful TO, allowing free material distribution within the design domain. In our optimization formulation, the domain is discretized by the quad elements and the density design variables varying from zeros to ones are assigned. Therefore, some structures that are hard to manufacture can appear after TO. Therefore, it is important to impose manufacturing constraints—here, piezoelectric rings with straight vertical lines should be designed. Compared with the size optimization, the total number of piezo rings is not limited in TO but the manufacturing constraints should be imposed. To do this, a morphology density filtering scheme to filter the design variables inside rectangular domains is implemented, as shown in Fig. 5.

The original density filtering is formulated as follows [12]:

$$\tilde{\gamma}_e = \frac{\sum_{i \in Neighbor} \omega(\mathbf{x}_i) \gamma_i}{\sum_{i \in Neighbor} \omega(\mathbf{x}_i) \gamma_i} \quad (23)$$

where the weighting function  $\omega(\mathbf{x}_i)$  is given by the linearly decaying function. The weight of the  $i$ th element is  $\gamma_i$ .

$$\omega(\mathbf{x}_i) = \max(0, r_{\min} - \|\mathbf{x}_i - \mathbf{x}_e\|), \quad \mathbf{x}_i = (r_i, z_i) \quad (24)$$

where the spatial coordinate value of  $\mathbf{x}_i$  in the axisymmetric system is  $\mathbf{x}_i = (r_i, z_i)$ . The filter radius is  $r_{\min}$ . In (24), the corn-shape function is considered. To obtain a smoother weighting function, the Gaussian distribution function can be used [36].

$$\omega(\mathbf{x}_i) = e^{-1/2(\|\mathbf{x}_i - \mathbf{x}_e\|/\sigma)^2}, \quad \sigma = r_{\min}/3, \quad \mathbf{x}_i = (r_i, z_i). \quad (25)$$

In the present paper, in order to impose the vertical manufacturing constraint, we propose to modify the above density filter as shown in Fig. 5 as follows:

$$\omega(\mathbf{x}_i) = \max(0, r_{\min} - \|r_i - r_e\|) \quad \text{with } \mathbf{x}_i = (r_i, z_i). \quad (26)$$

The weight factors of the elements in the vicinity only considering the radial direction are formulated in (26). With this modification, we found that the density filter method possesses the direction properties and the designs with this modified filter have vertical members only.



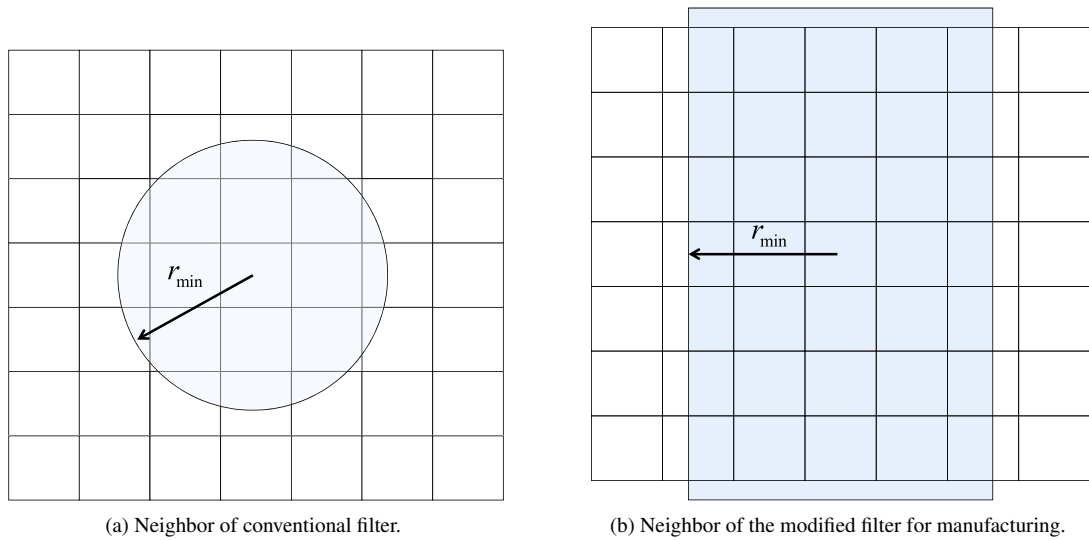


Fig. 5. Neighborhood element selection scheme.

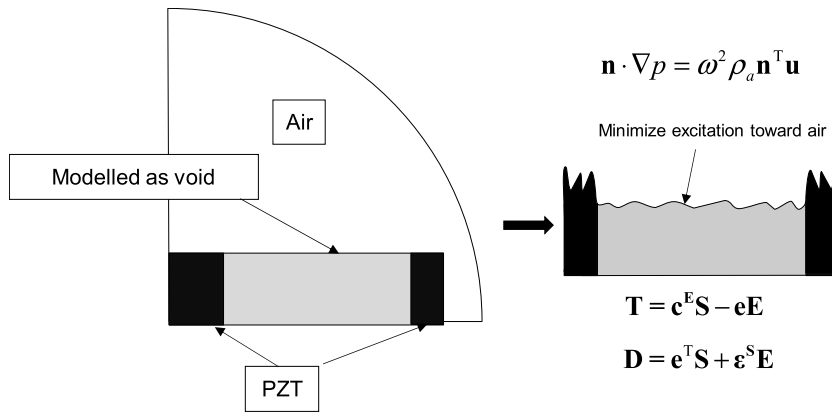


Fig. 6. The penalization factors minimizing excitation toward air domain.

Furthermore, the Dilate and Erode filters in [37] enforcing black and white optimal designs with the KS function are also implemented as follows:

$$\text{Dilate: } \tilde{\gamma}_e = \log \left( \frac{\sum_{i \in \text{Neighbor}} e^{\beta(\gamma_i)}}{\sum_{i \in \text{Neighbor}} 1} \right) / \beta \quad (27)$$

$$\text{Erode: } \tilde{\gamma}_e = 1 - \log \left( \frac{\sum_{i \in \text{Neighbor}} e^{\beta(1-\gamma_i)}}{\sum_{i \in \text{Neighbor}} 1} \right) / \beta \quad (28)$$

where the control parameter  $\beta$  is employed. The value is increased for every 20 iterations up to 200. Note that the set of the neighborhood elements is chosen as in Fig. 5(b). With the Erode filter, some detailed structures smaller than the radius or the box are not observed. As will be discussed later, the optimized designs obtained by the above filters are not sensitive to the variation of the design variables with low densities for the considered problem.

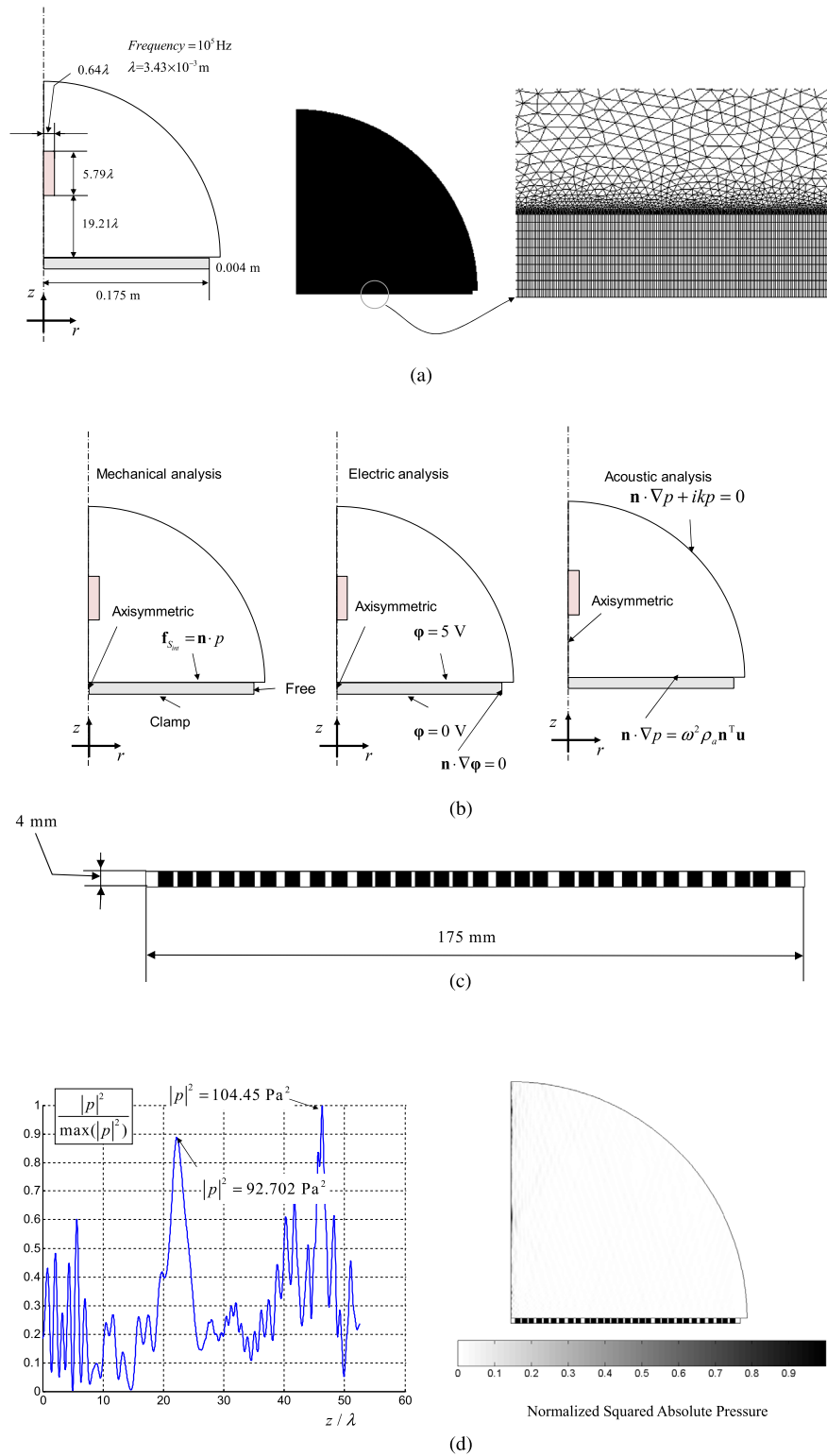


**Fig. 7.** Acoustic energy distribution of the focuser reference design [25]. (a) A problem definition and an axisymmetric finite element. (Total number of degrees of freedom: 783476, degrees of freedom of PZT: 378063, degrees of freedom of PZT: 405413.). (b) the boundary conditions, (c) the existing design and (d) the response.

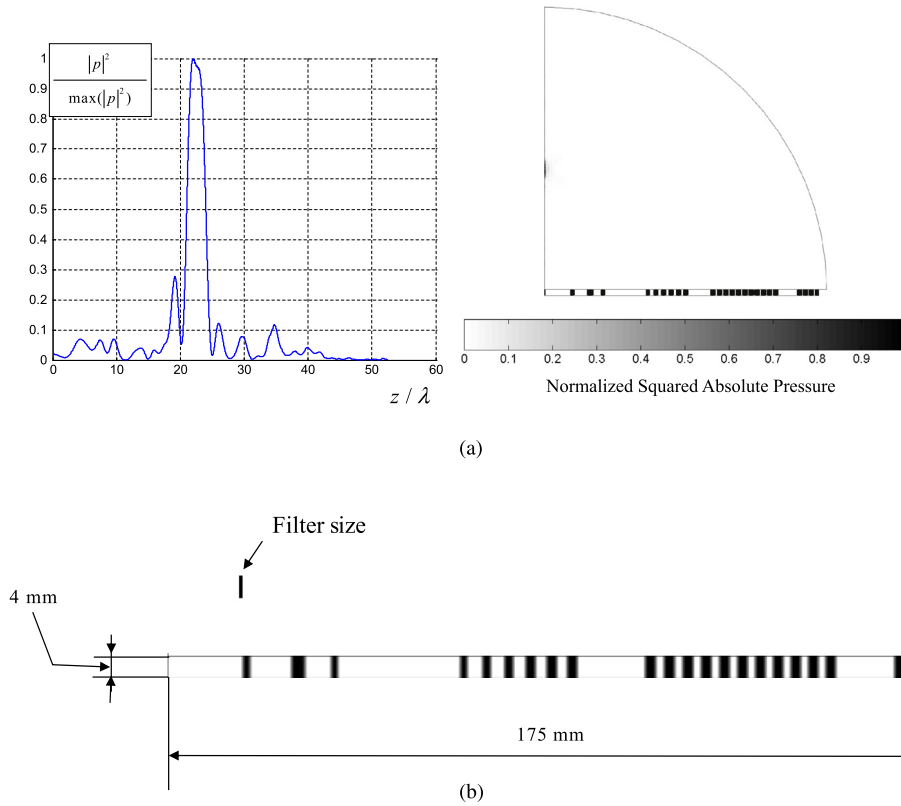


**Fig. 8.** Topology optimization result (the dilate density filter in (23),  $r_{\min}$ : 0.525 mm). ( $\max(|p|^2) = 842.71 \text{ Pa}^2$ ), Mass ratio = 30%. (a) Normalized squared absolute pressure and (b) detailed design.

### 3.2. Material interpolation

One of the difficulties involved in TO is that an optimization problem with a discrete design variable (zero or one) should be solved to determine solid domains (solid) or nonsolid domains (void) [11,12]. To cope with this difficulty, we usually introduce a continuous design variable to relax the optimization problem with a discrete design variable into an optimization problem with a continuous design variable varying from zero to one using simple polynomial functions.

To apply the SIMP-based interpolation functions to a piezoelectric material and the mass matrix, the following interpolation formulation can be adopted.

$$\begin{bmatrix} (\gamma_e)^{p_1} \mathbf{K}_{uu}^e & (\gamma_e)^{p_2} \mathbf{K}_{u\varphi}^e \\ (\gamma_e)^{p_2} \mathbf{K}_{\varphi u}^e & -(\gamma_e)^{p_3} \mathbf{K}_{\varphi\varphi}^e \end{bmatrix} \quad (0 < \gamma_e \leq 1) \quad (29)$$

$$(\gamma_e)^{p_4} \mathbf{M}_{uu}^e \quad (30)$$

where the penalization values for the structural stiffness, piezoelectric, permittivity and density matrices are  $p_1$ ,  $p_2$ ,  $p_3$  and  $p_4$ , respectively. In our simulation, we set these values as 3, 2, 7 and 5, respectively. Note that some combinations of different penalization values can be used with the density design variable of the  $e$ th element ( $\gamma_e$ ).

It is not problematic to model the piezoelectric ceramic with ones for the design variables. However, some care should be taken for the domain with zero design variables. Along the boundaries between the piezoelectric material domain and the void domain with zero design variables, the zero-traction boundary conditions should be imposed on the mechanical equation and the zero-charge boundary condition should be imposed on the electric equation. The hard boundary condition should be imposed at the top boundaries of the void domain. This means that the stiffness ratio of

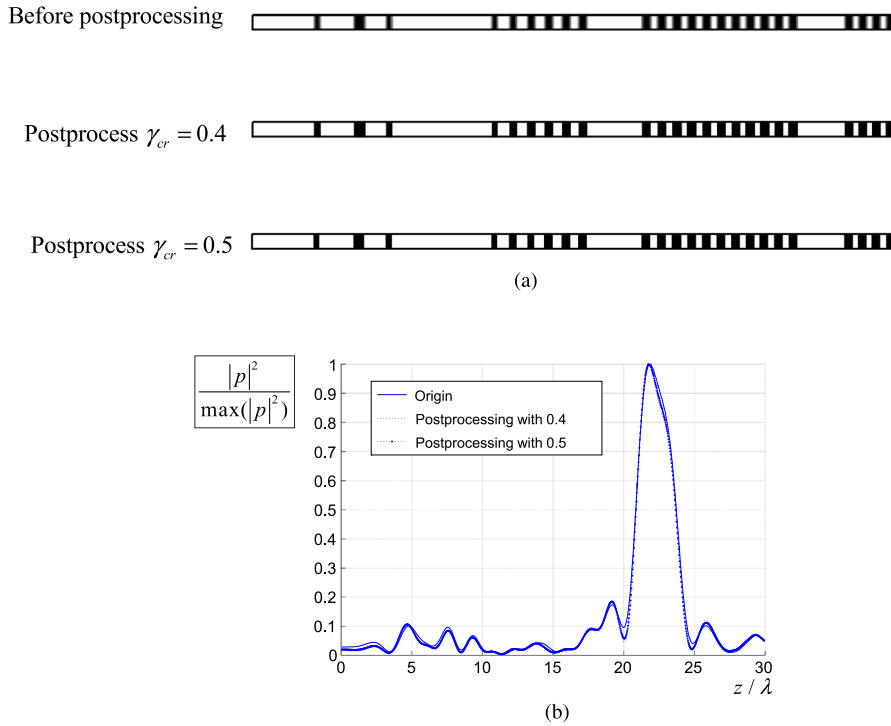


Fig. 9. Hard-kill postprocessing in SIMP ( $\max(|p|^2) = 842.71 \text{ Pa}^2$ ).

the piezo domain and the void domain should be so large that the stiffness of the void domain should be negligible. However, the displacements of the top boundaries of the void domain should converge to zero for the hard boundary condition. In our numerical tests, the ratio can be controlled by the lower bound of the design variables.

In choosing the penalization factors, the excitation of the PZT area modeled as void region should be minimized so as not to make artificial acoustic energy as shown in Fig. 6. The excitation toward air domain is formulated by (14), i.e.,  $\mathbf{n} \cdot \nabla p = \omega^2 \rho_a \mathbf{n}^T \mathbf{u}$ . Due to the voltage boundary condition at the top and the bottom surfaces of PZT, the electric field,  $\mathbf{E}$ , does not vanish although the lower design value, here 0.001, is assigned. In the coupling equations (1), we found that the large stress and the associate large displacements can occur with some improper combinations of the penalization factors; note that the stored elastic structural energy in the void region is still small. In the coupling equations (1), it is our conclusion that the higher penalization value for the structural constitutive matrix,  $\mathbf{c}^E$ , should be prevented. Furthermore, the “local vibration mode” should be prevented at the PZT region modeled as void. Therefore, a higher penalization factor for the mass matrix is chosen. Because some side effects can happen after an optimization, the postprocessing of the optimized layouts and the reanalysis without the PZT region modeled as void region should be carried out to check the validity of the optimized result.

#### 4. Topology optimization result

To validate the usefulness and performance of the developed optimization theory, the layouts of the acoustic energy focusers are optimized with different frequencies. It shows that the developed optimization formulation is able to present some optimized topologies whose performances are better than those presented in the existing literatures. The geometry and boundary conditions are chosen by the references so as to show the potential application of the abovementioned theory.

**Example 1.** Acoustic focuser, Excitation Frequency = 100,000 Hz.

To show the validity of the present study, the acoustic focuser problem in [25], which is a pioneering work in this research field, is considered. The design domain is the piezoelectric bottom box ( $0.175 \text{ m} \times 0.004 \text{ m}$ ) and the

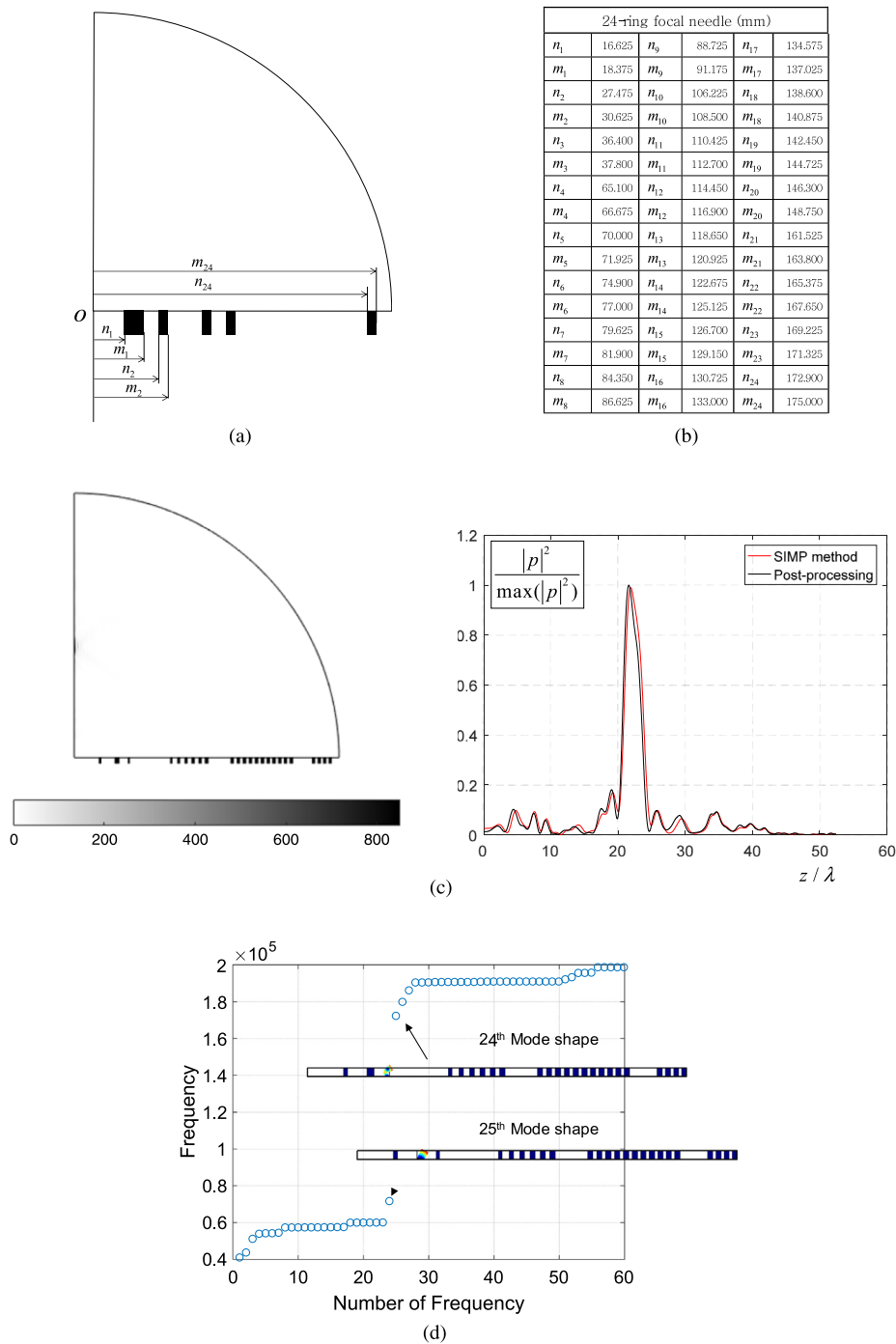


**Fig. 10.** Hard-kill postprocessing in CAD.

acoustic domain above the piezoelectric bottom box is coupled with the piezoelectric bottom box. With an electric excitation, the piezoelectric structure vibrates and it induces the acoustic fluctuation or the acoustic energy as shown in Fig. 7(b). This becomes an engineering problem to determine the piezoelectric rings required to manipulate the acoustic energy to a certain designated area. In this engineering problem, the energy distribution should be considered;

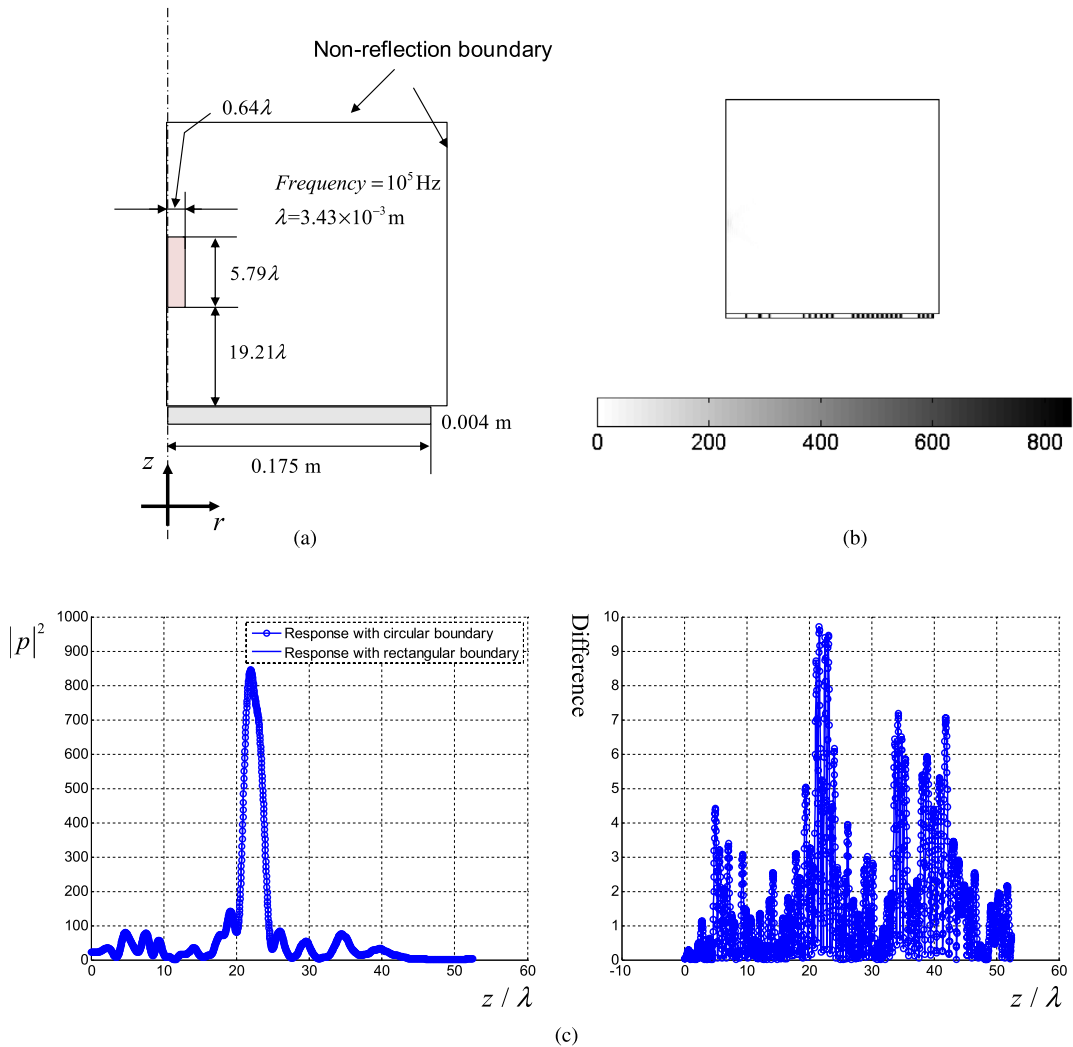


**Fig. 11.** Reanalysis of the design of Fig. 8 with the rectangular non-reflection boundary condition. (a) The rectangular boundary condition, (b) the response and (c) the response and the comparison.

the acoustic energy should be focused at the designated area and the acoustic energy outside of the designated area should be minimized. This minimization of the acoustic energy outside the designated area is important in maximizing a medical treatment in the designated area and minimizing tissue damage elsewhere. Moreover, it is better to maximize the acoustic energy at the designated area to have a cost-effective device.

As a reference, the design with 30 rings in [25] is reanalyzed with the developed axisymmetric FE code in Fig. 7. The pressure distribution along the symmetric line is shown in Fig. 7. This size-optimized design is proposed in [25] by applying a meta heuristic optimization method and maximizing the pressure at the objective domain ( $5.79\lambda \times 0.64\lambda$ ), where the wavelength is denoted by  $\lambda$ . As shown in Fig. 7(d), the acoustic energy generated by the piezoelectric rings is successfully focused at the objective domain. However, the acoustic energy distribution from the surface of the piezoelectric rings to 10 times of the wavelength in the  $z$ -coordinate is not even and oscillating up to 0.7 times of the maximum acoustic energy of the objective domain. This becomes serious after 40 times of the wavelength in the  $z$ -coordinate. This oscillation and the peak inevitably cause tissue damages and prohibit us from increasing the excitation voltage. After 40 times of the wavelength, some high-pressure peaks are also observed.

Fig. 8 shows the topology optimization result with the present approach. The design domain is discretized by 3000 by 10 elements. The initial density distribution is set to 0.5 and the optimization process is carried out for the design

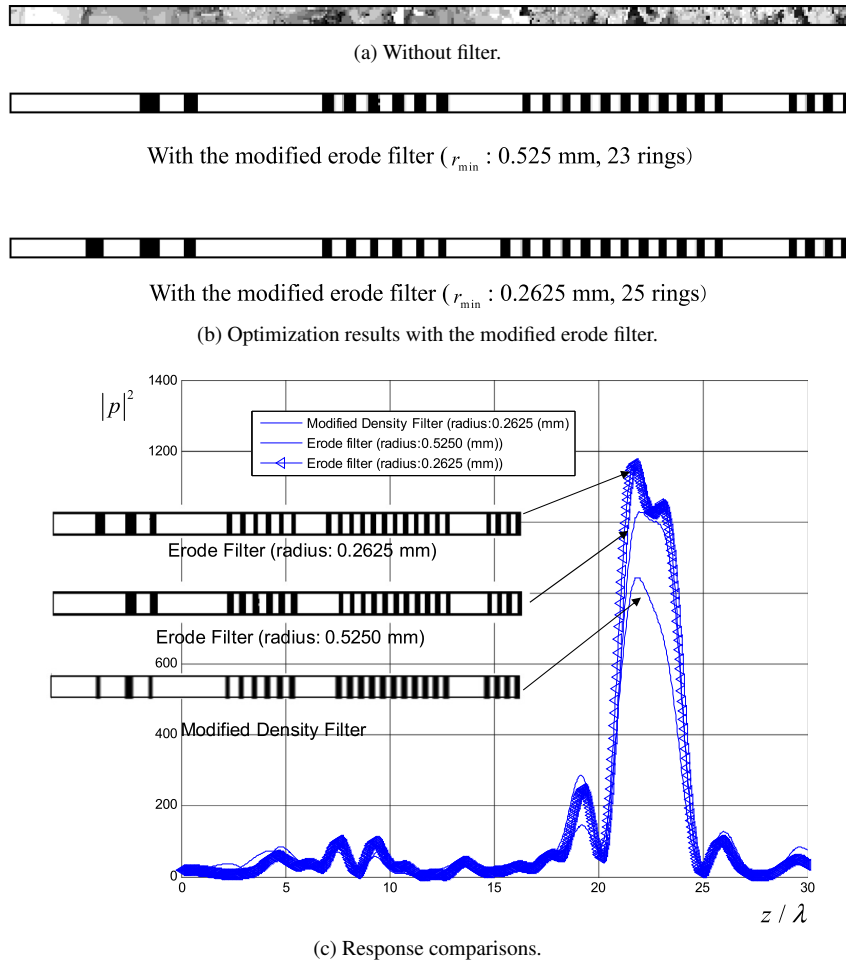


**Fig. 12.** Designs by modified morphology filter. (a) Result without the modified filter, (b)–(c) results with the modified filter and the response comparison.

in Fig. 8. With the present topology optimization method, the design with 24 rings in Fig. 8(b) can be obtained with  $r_{\min} = 0.525$  mm for the radius of the density filter. The piezoelectric ring design has three rings near the axis line, six rings after one gap, 11 rings with the almost equal sizes after another gap, and four rings after the other gap. Owing to this density dilate filter, some gray design variables exist. Note that the maximum pressure is increased to  $\max(|p|^2) = 842.71 \text{ Pa}^2$ .

The design of Fig. 8 is superior to the design optimized by the size optimization in terms of the performance. However, some gray design variables exist, which is one of the characteristics and disadvantages of the TO. To study the effect of these gray design variables, the hard-kill postprocessing (setting 1 or the lower bound (0.001) depending on a criterion value ( $\gamma_{cr}$ )) is applied in Fig. 9. The responses and objective values are not different for the hard-kill postprocess.

Furthermore, the hard-kill postprocessing in CAD is applied in Fig. 10. Here there is no artificial material in void regions. As illustrated, the responses are similar to each other that shows the validity of the present formulation.

During an optimization, some resonances of the PZT rings can occur. From an optimization problem, these resonances can cause some oscillations during an optimization. For an example, Fig. 10(d) shows the first 60 eigenvalues of the PZT rings. Near the excitation frequency, the bending modes of the second ring and the third ring are observed. If the resonance frequencies of the PZT rings are matched with the excitation frequency ( $10^5 \text{ Hz}$ ), the displacements of the PZT rings can become infinite. In our numerical test, it is not problematic. If this issue becomes serious, some damping in the constitutive matrix can be included.

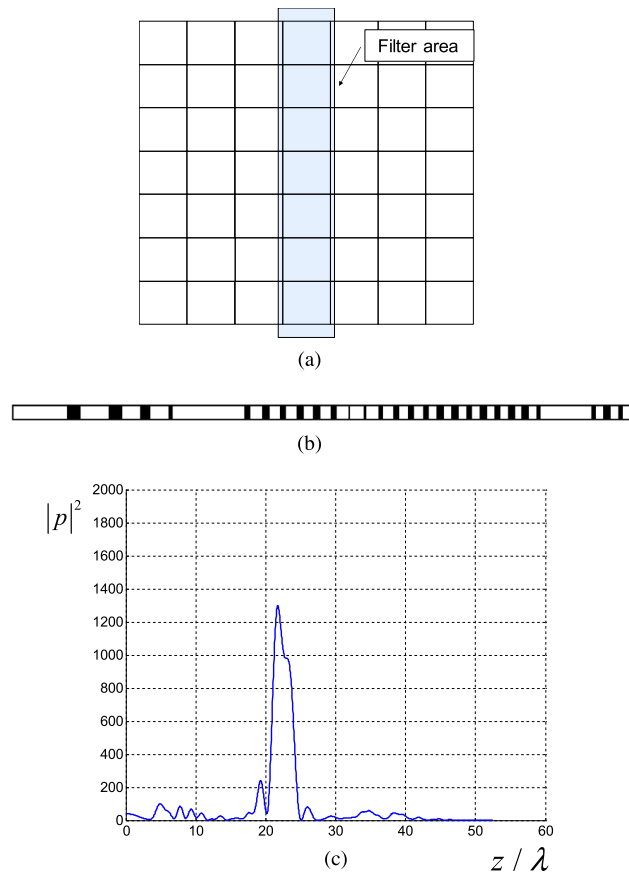


**Fig. 13.** A 1-dimensional design discretization with the modified filter box.

From the discussion,<sup>1</sup> it was noticed that with some objects reflecting acoustic wave at the boundary of the quadrant of the acoustic domain, some different optimized designs can be obtained. Thus, it was also noticed that the no-reflection boundary condition should be checked because the accuracy of the non-reflection boundary condition will affect the accuracy of the analysis and the optimization result. To model the infinite boundary, it is important to have a sufficiently large space to minimize the effect of the reflected wave. In order to check this, we modify the circular shape boundary to the rectangular boundary as shown in Fig. 11 and calculate the responses of the design in Fig. 8 for the rectangular acoustic domain in Fig. 11. The responses of the circular domain and the rectangular domain are similar.

For the sake of the complete discussions about the effect of the density filters in topology optimization, Fig. 12 shows the several layouts. Owing to the local optimality, a fuzzy layout with a bad objective value is obtained without the regulation. With the erode filter, it is possible to obtain the clear layouts in Fig. 12(b), which implies that the present TO requires the regulation method to overcome the complex function space and the local optima issue. Fig. 12(c) shows the responses of the designs and the responses by the modified erode filter actually works well in terms of the regulation in topology optimization. From the discussion,<sup>2</sup> it was noticed that the method with a single design variable for each column of elements or as a 1-dimensional design discretization can be implemented by modifying the shape of the modified filter. With this optimization formulation with one dimensional design discretization, we could obtain the following design of Fig. 13 without considering the manufacturability. Because the design space is enlarged but sufficiently limited to remove the local optima issue, another local optimum can be obtained and the performance is also enhanced. However, the member sizes of some PZT rings are too small to be manufactured.

<sup>1</sup> A comment by an anonymous reviewer.

<sup>2</sup> A comment by an anonymous reviewer.



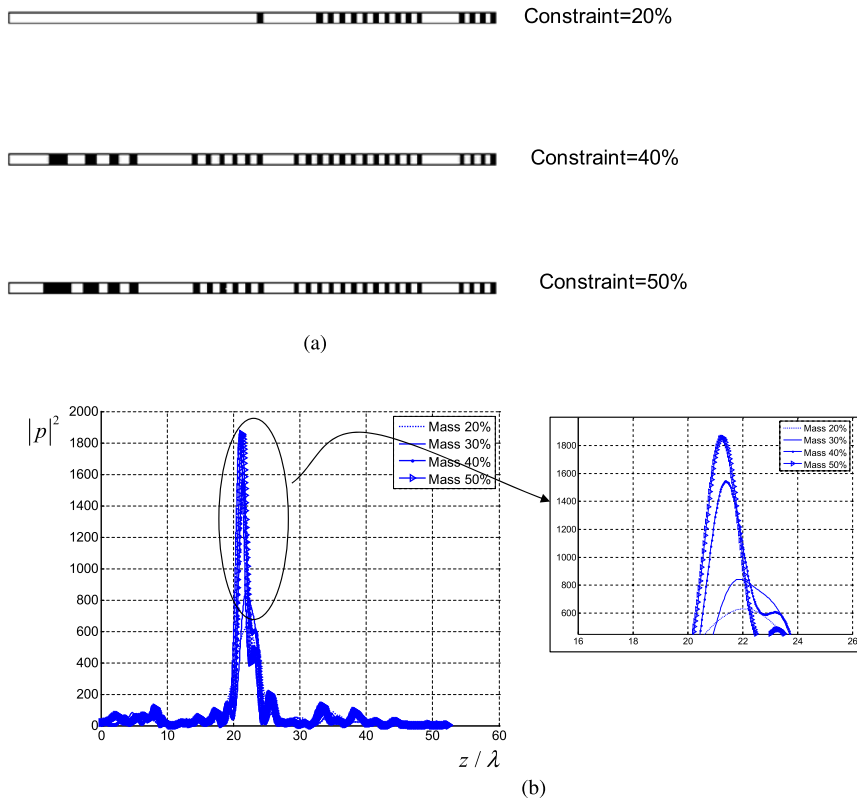


**Fig. 14.** Designs with different mass usage (Modified erode filter:  $r_{\min}$ : 0.525 mm).

For the above optimization results, the 30% mass constraint is imposed. In Fig. 14, the influence of the mass variation is tested. Because the actuation energy increases with more PZT material, higher acoustic energy focusing can be achievable.

During the optimizations, it was observed that some designs showing straight acoustic beam can be obtained. It is because the present optimization formulation (18) does not consider the pressure peak at the domain excluding the object domain. One of the best designs of the present formulation without the mass constraint and the constraint preventing undesired pressure peak is a cylinder design showing the straight acoustic beam. For an example, in the case of 50% mass in Fig. 14, after 130 iterations, we initially could obtain a converged design. However, when we continue the design process neglecting our convergence criterion, the design shown in Fig. 15 can be obtained. In terms of the objective function, its response at the objective domain is much higher. However, it is impractical to use this design because the pressure peak at the domain excluding the object domain is also high. Thus, it is necessary to insert the constraint preventing undesired pressure peak. For the sake of this, the extra constraint preventing undesired pressure peak can be included as follows:

$$\begin{aligned}
 & \text{Max}_{\gamma} \int_{\Omega_{obj}} |p| dv (\Omega_{obj} : \text{an objective domain}) \\
 & \text{Subject to } \sum_{e=1}^{NED} \gamma_e v_e \leq V^* \\
 & \int_{\tilde{\Omega}} |p| dv \leq \alpha_{tolerance} \int_{\Omega_{obj}} |p| dv (\tilde{\Omega} : \text{acoustic domain except } \Omega) \\
 & \tilde{\gamma} = filter(\gamma).
 \end{aligned} \tag{31}$$

Note that the second constraint preventing undesired pressure peak is added in the above formulation. The scaling factor is  $\alpha_{tolerance}$ . With the above optimization formulation, the unwanted peak can be prevented as shown in Fig. 16.

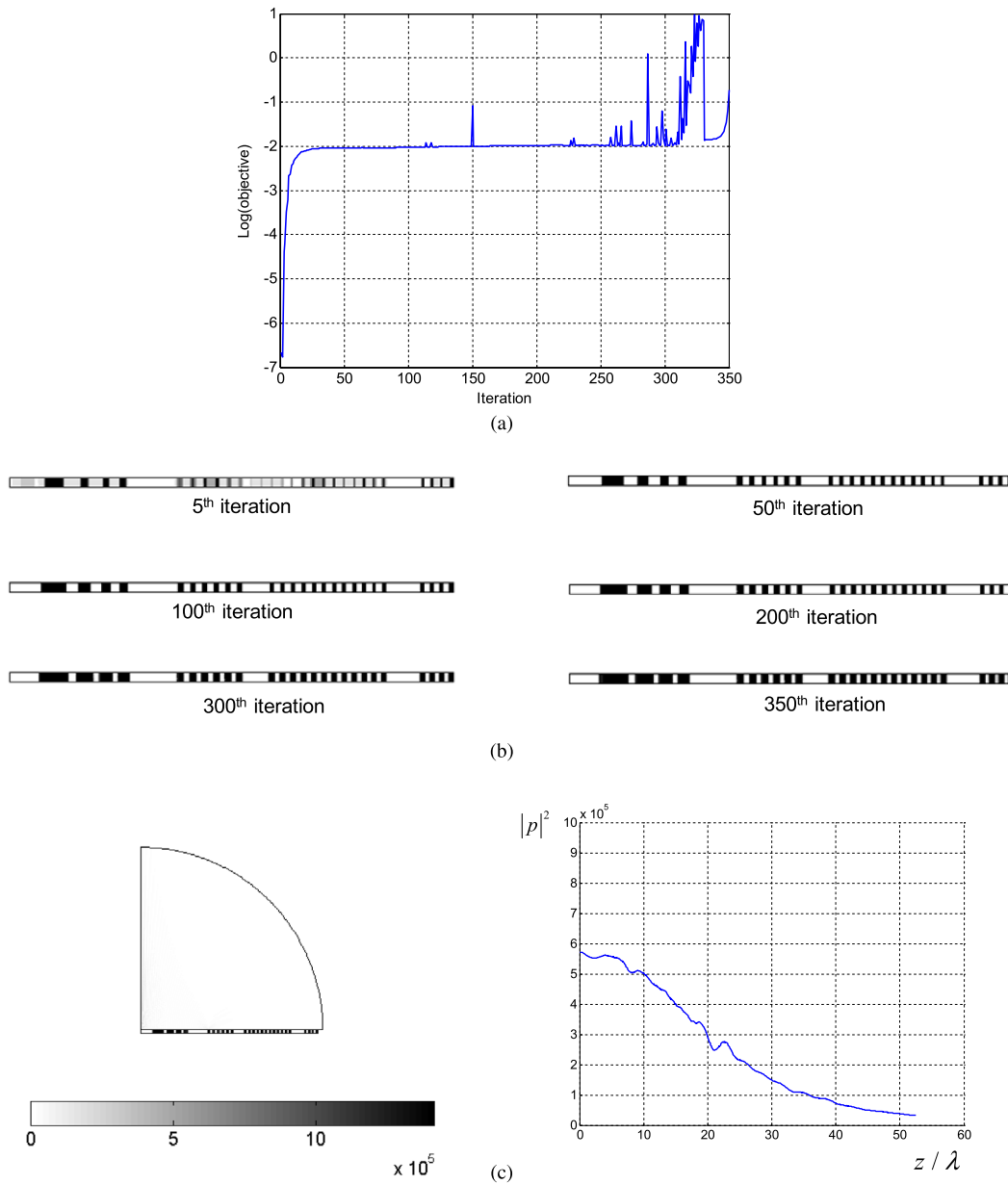


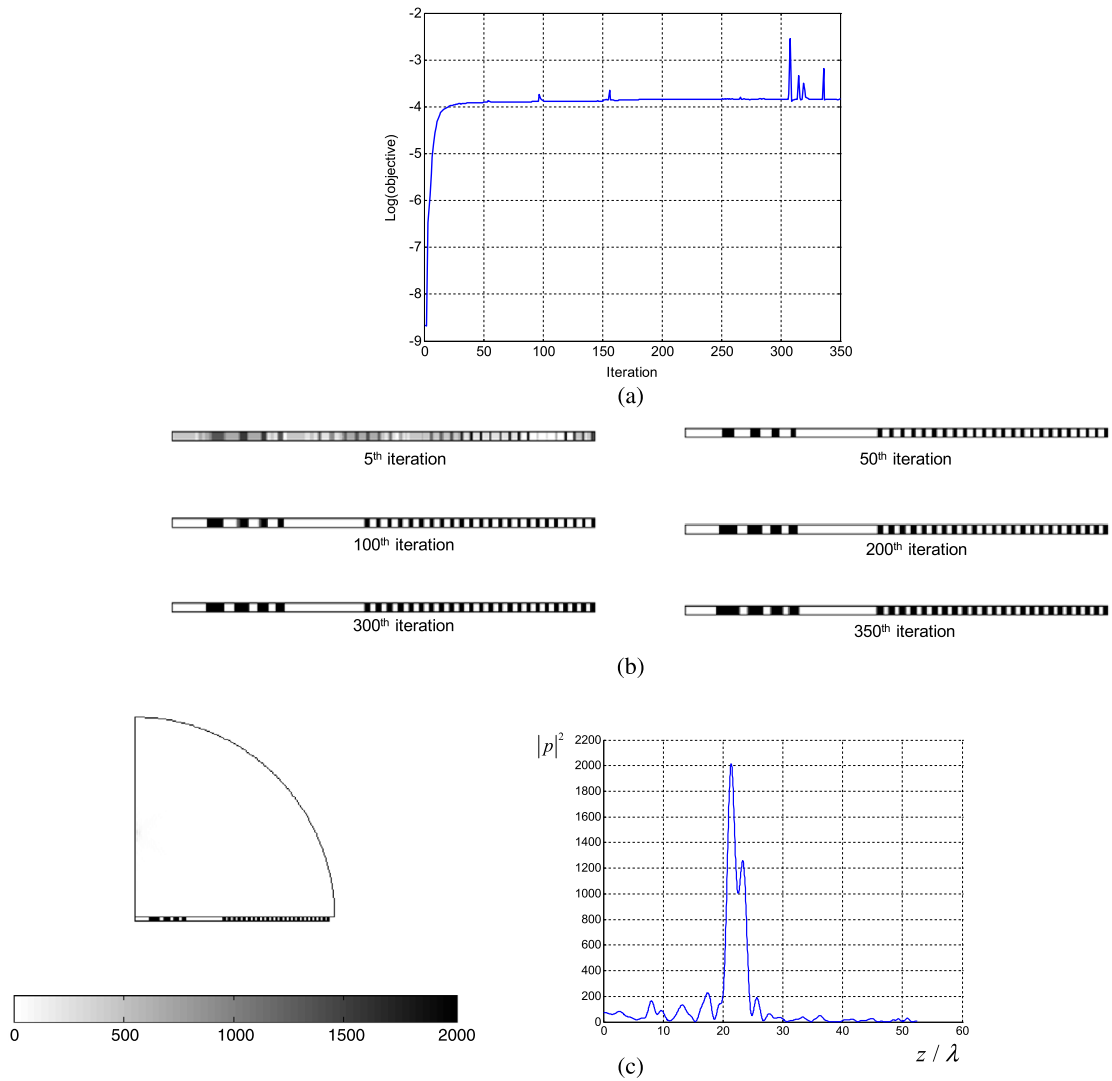
**Fig. 15.** A design history with 50% mass usage; the straight beam design. (a) An optimization history, modified erode filter  $r_{\min}$ : 0.525 mm), (b) some designs and (c) straight beam (unwanted focused beam).

### Example 2. Acoustic focuser with different excitation frequencies.

To test the effect of the excitation frequency, the designs with different excitation frequencies are presented in Figs. 17 and 18. The designs in Figs. 17 and 18 and that in Fig. 8 imply that by increasing the excitation, the space between the piezoelectric rings and the widths of the piezo rings becomes narrow and small. The wavelength of the acoustic wave is increased and the envelope of the focused acoustic energy is widened and smoothed.

### Example 3. Acoustic focuser with two focal zones.

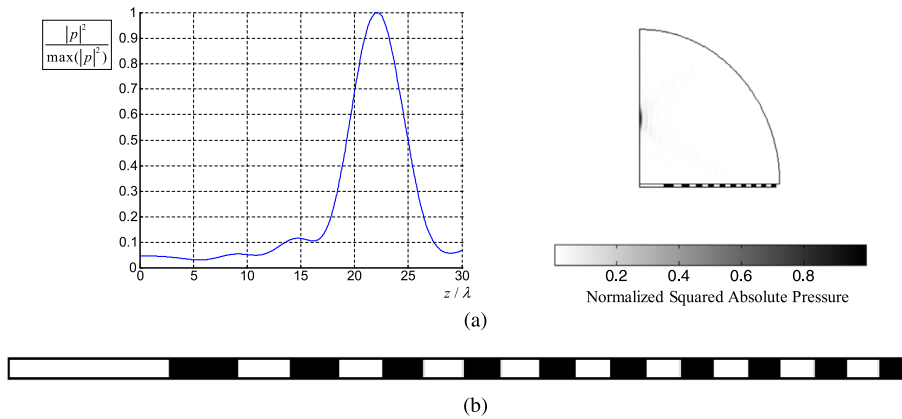
For the next example, the TO to maximize the focused acoustic energies at the two areas in Fig. 19 is considered. At the above the bottom electrode, the two rectangular areas are preselected as the energy focusing areas. For a TO



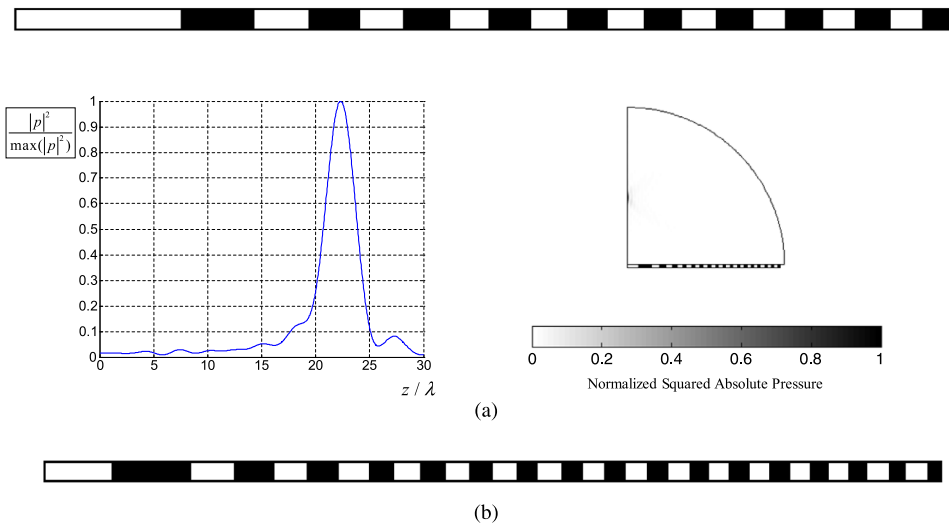
**Fig. 16.** A design history with 50% mass usage and the constraint removing unwanted focused beam. ( $\alpha_{tolerance} = 2$ ) (a) An optimization history, modified erode filter  $r_{min}$ : 0.525 mm), (b) some designs and (c) pressure distributions.

formulation, the sum of the objective functions at the two design domains ( $\Omega_1$  and  $\Omega_2$ ) is maximized with the mass constraint and the difference constraint. As the magnitudes of the integrals of the acoustic energy at the objective domains vary significantly, the sum of the ratios of the two acoustic integrals is constrained with an allowable value,  $\varepsilon^*$ .

$$\begin{aligned}
 & \text{Max}_{\gamma} \int_{\Omega_1} |p| dv + \int_{\Omega_2} |p| dv \\
 & \text{Subject to } \sum_{e=1}^{NED} \gamma_e v_e \leq V^* \\
 & \left( \frac{\int_{\Omega_1} |p| dv}{\int_{\Omega_2} |p| dv} - 1 \right)^2 + \left( \frac{\int_{\Omega_2} |p| dv}{\int_{\Omega_1} |p| dv} - 1 \right)^2 \leq \varepsilon^* (\varepsilon^* = 0.1) \\
 & \tilde{\gamma} = filter(\gamma).
 \end{aligned} \tag{32}$$



**Fig. 17.** Topology optimization result (Modified erode filter  $r_{\min}$ : 0.525 mm,  $\max(|p|^2) = 13.9375 \text{ Pa}^2$ , excitation frequency = 30,000 Hz), Mass ratio = 80%. (a) Normalized squared absolute pressure and (b) detailed design (10 rings).



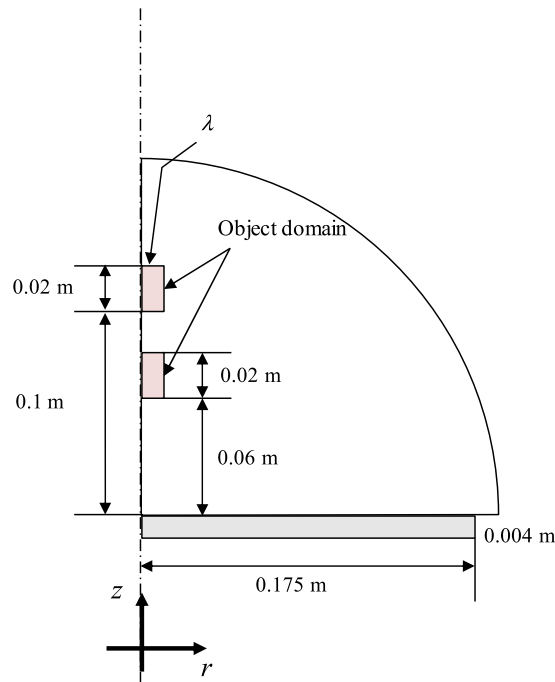
**Fig. 18.** Topology optimization result (Modified erode filter  $r_{\min}$ : 0.525 mm,  $\max(|p|^2) = 123.1770 \text{ Pa}^2$ , excitation frequency = 50,000 Hz), Mass limit = 80%, (a) Normalized squared absolute pressure and (b) detailed design (17 rings).

Fig. 20 shows an optimized topology for 30 kHz and the associated acoustic energy distributions. As illustrated, an optimized topology increasing the acoustic energy at the two domains can be obtained. The gray elements are postprocessed in Fig. 21 and it shows that the presented optimization process can determine an optimized topology successfully.

Fig. 22 shows an optimized topology for 100,000 Hz and the associated acoustic energy distributions. It is possible to successfully obtain an optimized piezoelectric structure with the present approach. Because the wavelength is decreased, sharp energy focusing is possible with the present approach. With the modified erode filter, the gray element issue is significantly lessened, but the hard-kill postprocessing is applied at Fig. 23 to check the gray element issue.

## 5. Conclusions

This research presents a new TO framework for piezoelectric devices to focus acoustic energy. For this purpose, the axisymmetric multiphysics FE simulation for the piezoelectric domain and acoustic domain is used. To overcome the nonconvergence to black and white design and to consider the manufacturing constraints, the modified density filter and the erode morphing filter are implemented. Specifically, to have the vertically nonvarying piezoelectric structure, a



**Fig. 19.** Acoustic energy focuser at two domains.

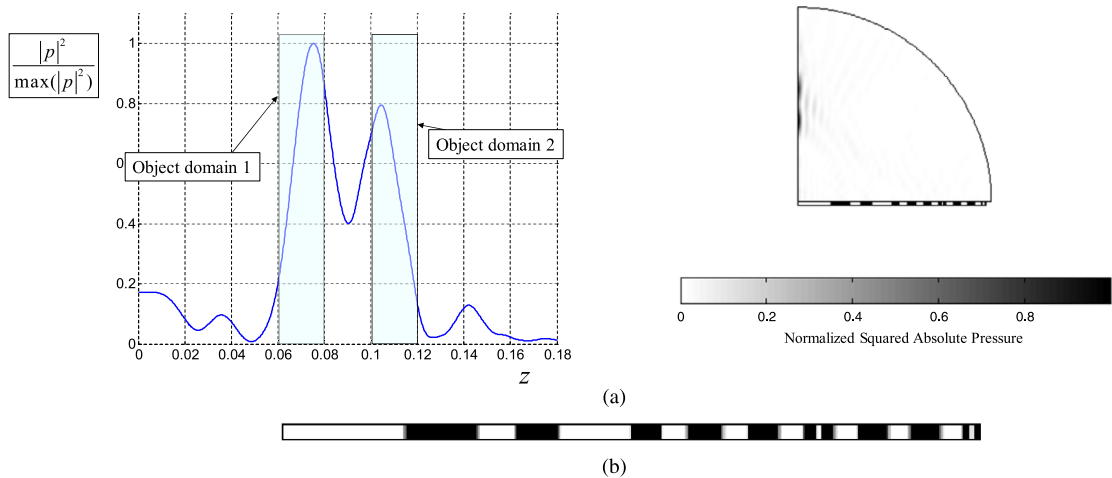


**Fig. 20.** Topology optimization result with the modified erode filter ( $\max(|p|^2) = 6.1055 \text{ Pa}^2$ , excitation frequency = 30,000 Hz), mass usage = 51.79%). (a) Normalized squared absolute pressure and (b) detailed design.

box with an infinite size in the vertical direction is used in defining the neighborhood elements. With the density filter methods considering the manufacturability, the optimization formulation maximizing the squared absolute pressure at the target domain subject to mass constraint is considered.

For the material interpolation for the optimization problem, the SIMP approach interpolating the constitutive matrix for the piezoelectric material with respect to the density variable is employed here. The configurations of the piezoelectric materials that are solutions of the optimization problem confirm that the domain and boundary configurations play an important role in the distributions of the extension and compression stresses within a piezoelectric material. Compared to the structure optimized by the size optimization framework with fixed piezo

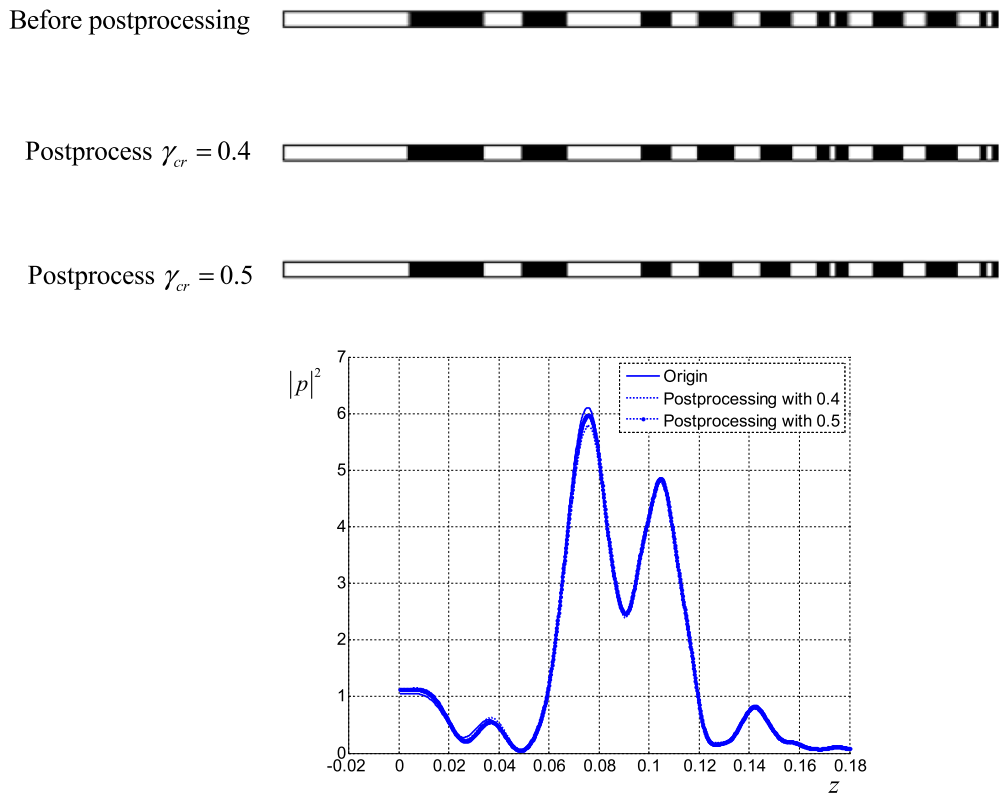


Fig. 21. Hard-kill postprocessing.

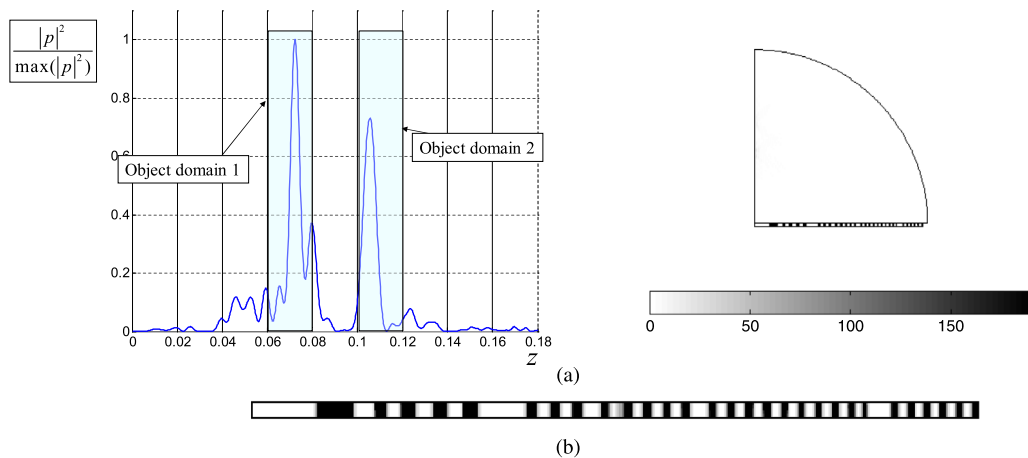


Fig. 22. Topology optimization result with the modified Erode filter ( $\max(|p|^2) = 6.1055 \text{ Pa}^2$ , excitation frequency = 100,000 Hz, Mass usage = 31.76%). (a) Normalized squared absolute pressure and (b) detailed design.

rings, the TO structures show better performances. By investigating the optimization results, it is observed that by increasing the excitation frequency, the number of piezoelectric rings is also increased. With the TO framework, the number, sizes, and locations of piezoelectric rings are found after the optimization process. However, we should mention that the designs in the present study are local optima but they show better performances than those of the designs optimized by the size optimization process.

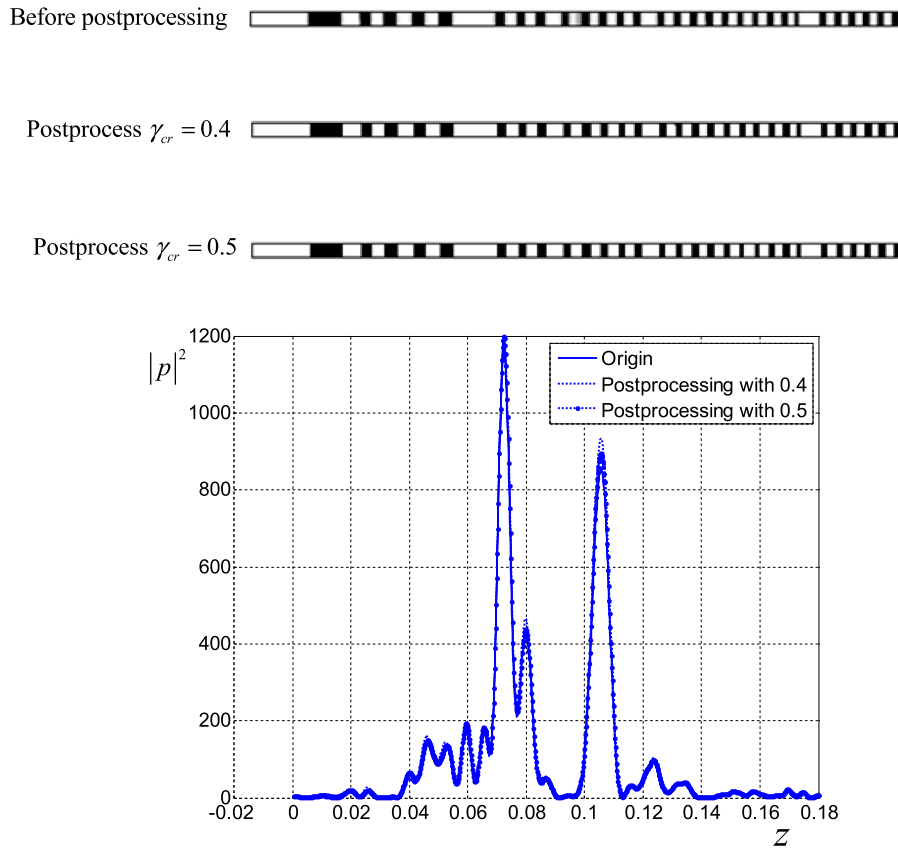


Fig. 23. Hard-kill postprocessing.

## Acknowledgment

This work was supported by the National Research Foundation of Korea (NRF) Grant [No: 2014M3A6B3063711 (Global Frontier R&D Program on Center for Wave Energy Control based on Metamaterials)] funded by the Korean Ministry of Science, ICT and Future Planning (MSIP).

## References

- [1] A. Meitzler, H. Tiersten, A. Warner, D. Berlincourt, G. Couquin, F. Welsh III, IEEE standard on piezoelectricity, in, Society, 1988.
- [2] C.J. Rupp, A. Evgrafov, K. Maute, M.L. Dunn, Design of piezoelectric energy harvesting systems: a topology optimization approach based on multilayer plates and shells, *J. Intell. Mater. Syst. Struct.* 20 (2009) 1923–1939.
- [3] E.C.N. Silva, N. Kikuchi, Design of piezoelectric transducers using topology optimization, *Smart Mater. Struct.* 8 (1999) 350.
- [4] E.C.N. Silva, S. Nishiwaki, N. Kikuchi, Design of piezocomposite materials and piezoelectric transducers using topology optimization—part II, *Arch. Comput. Methods Eng.* 6 (1999) 191–215.
- [5] E.N. Silva, J.O. Fonseca, F.M. de Espinosa, A. Crumm, G. Brady, J. Halloran, N. Kikuchi, Design of piezocomposite materials and piezoelectric transducers using topology optimization—part I, *Arch. Comput. Methods Eng.* 6 (1999) 117–182.
- [6] E.N. Silva, S. Nishiwaki, N. Kikuchi, Topology optimization design of flexensional actuators, *IEEE Trans. Ultrason. Ferroelectr. Freq. Control* 47 (2000) 657–671.
- [7] H.A. Sodano, D.J. Inman, G. Park, A review of power harvesting from vibration using piezoelectric materials, *Shock Vib. Dig.* 36 (2004) 197–206.
- [8] Z. Luo, L. Tong, J. Luo, P. Wei, M.Y. Wang, Design of piezoelectric actuators using a multiphase level set method of piecewise constants, *J. Comput. Phys.* 228 (2009) 2643–2659.
- [9] W.J. McCalla, *Fundamentals of Computer-Aided Circuit Simulation*, Kluwer Academic Publishers, Norwell, 1988.
- [10] H. Allik, T.J. Hughes, Finite element method for piezoelectric vibration, *Internat. J. Numer. Methods Engrg.* 2 (1970) 151–157.

- [11] M.P. Bendsøe, N. Kikuchi, Generating optimal topologies in structural design using a homogenization method, *Comput. Methods Appl. Mech. Engrg.* 71 (1988) 197–224.
- [12] M.P. Bendsoe, O. Sigmund, *Topology Optimization: Theory, Methods, and Applications*, Springer, Berlin, 2003.
- [13] S. Canfield, M. Frecker, Topology optimization of compliant mechanical amplifiers for piezoelectric actuators, *Struct. Multidiscip. Optim.* 20 (2000) 269–279.
- [14] R.C. Carbonari, E.C. Silva, S. Nishiwaki, Optimum placement of piezoelectric material in piezoactuator design, *Smart Mater. Struct.* 16 (2007) 207.
- [15] B. Zheng, C.-J. Chang, H.C. Gea, Topology optimization of energy harvesting devices using piezoelectric materials, *Struct. Multidiscip. Optim.* 38 (2009) 17–23.
- [16] R.C. Carbonari, E.C. Silva, G.H. Paulino, Multi-actuated functionally graded piezoelectric micro-tools design: A multiphysics topology optimization approach, *Internat. J. Numer. Methods Engrg.* 77 (2009) 301–336.
- [17] S. Chen, S. Gonella, W. Chen, W.K. Liu, A level set approach for optimal design of smart energy harvesters, *Comput. Methods Appl. Mech. Engrg.* 199 (2010) 2532–2543.
- [18] J.S. Choi, J. Yoo, Simultaneous structural topology optimization of electromagnetic sources and ferromagnetic materials, *Comput. Methods Appl. Mech. Engrg.* 198 (2009) 2111–2121.
- [19] Z. Kang, L. Tong, Topology optimization-based distribution design of actuation voltage in static shape control of plates, *Comput. Struct.* 86 (2008) 1885–1893.
- [20] J.E. Kim, D.S. Kim, P.S. Ma, Y.Y. Kim, Multi-physics interpolation for the topology optimization of piezoelectric systems, *Comput. Methods Appl. Mech. Engrg.* 199 (2010) 3153–3168.
- [21] M. Kögl, E.C. Silva, Topology optimization of smart structures: design of piezoelectric plate and shell actuators, *Smart Mater. Struct.* 14 (2005) 387.
- [22] J. Zhai, G. Zhao, L. Shang, Integrated design optimization of structural size and control system of piezoelectric curved shells with respect to sound radiation, *Struct. Multidiscip. Optim.* (2017).
- [23] F. Wein, M. Kaltenbacher, E. Bänsch, G. Leugering, F. Schury, Topology optimization of a piezoelectric-mechanical actuator with single-and multiple-frequency excitation, *Int. J. Appl. Electromagn. Mech.* 30 (2009) 201–221.
- [24] J.Y. Noh, G.H. Yoon, Topology optimization of piezoelectric energy harvesting devices considering static and harmonic dynamic loads, *Adv. Eng. Softw.* 53 (2012) 45–60.
- [25] J.J. Zhao, H.P. Ye, K. Huang, Z.N. Chen, B.W. Li, C.W. Qiu, Manipulation of acoustic focusing with an active and configurable planar metasurface transducer, *Sci. Rep.-UK* 4 (2014).
- [26] S. Zhai, H. Chen, C. Ding, F. Shen, C. Luo, X. Zhao, Manipulation of transmitted wave front using ultrathin planar acoustic metasurfaces, *Appl. Phys. A* 120 (2015) 1283–1289.
- [27] G.H. Yoon, Topology optimization for stationary fluid–structure interaction problems using a new monolithic formulation, *Internat. J. Numer. Methods Engrg.* 82 (2010) 591–616.
- [28] M.B. Dühring, J.S. Jensen, O. Sigmund, Acoustic design by topology optimization, *J. Sound Vib.* 317 (2008) 557–575.
- [29] G.H. Yoon, Acoustic topology optimization of fibrous material with Delany-Bazley empirical material formulation, *J. Sound Vib.* 332 (2013) 1172–1187.
- [30] H. Jensen, *Calculations for Piezoelectric Ultrasonic Transducers in*, Risø National Laboratory, Risø National Laboratory, DK-4000 Roskilde, Denmark, 1986.
- [31] K. Bathe, *Finite Element Procedures*, Prentice Hall, New Jersey, 1996.
- [32] R.D. Cook, D.S. Malkus, M.E. Plesha, R.J. Witt, *Concepts and Applications of Finite Element Analysis*, John Wiley & Sons, New Jersey, USA, 2001.
- [33] M.Y. Shatalov, A.G. Every, A.S. Yenwong-Fai, Analysis of non-axisymmetric wave propagation in a homogeneous piezoelectric solid circular cylinder of transversely isotropic material, *Internat. J. Solids Struct.* 46 (2009) 837–850.
- [34] E. Deckers, D. Vandepitte, W. Desmet, A Wave Based Method for the axisymmetric dynamic analysis of acoustic and poroelastic problems, *Comput. Methods Appl. Math.* 257 (2013) 1–16.
- [35] K. Svanberg, The method of moving asymptotes—a new method for structural optimization, *Internat. J. Numer. Methods Engrg.* 24 (1987) 359–373.
- [36] T.E. Bruns, D.A. Tortorelli, An element removal and reintroduction strategy for the topology optimization of structures and compliant mechanisms, *Internat. J. Numer. Methods Engrg.* 57 (2003) 1413–1430.
- [37] O. Sigmund, Morphology-based black and white filters for topology optimization, *Struct. Multidiscip. Optim.* 33 (2007) 401–424.